Sensors and Materials, Vol. 28, No. 1 (2016) 43–54
MYU Tokyo

S & M 1155

Application of Single-Crystalline N-type and P-type ZnO Nanowires in Miniaturized Gas Ionization Sensor

Svetlana Spitsina* and Mojtaba Kahrizi

Department of Electrical and Computer Engineering, Concordia University,
1515 St. Catherine West, S-EV005.139, Montreal, Quebec, Canada, H3G 2W1

(Received May 1, 2015; accepted July 21, 2015)

Keywords: Ag-doped ZnO nanowires, breakdown voltage, gas ionization sensor, field enhancement factor

Gas ionization sensors (GISs) based on n-type and p-type ZnO nanowires (NWs) have been fabricated and successfully tested in field ionization (FI) and field emission (FE) modes in sub-Torr atmospheres of various gases (Ar, He, N_2, and O_2). Novel GISs demonstrated good stability and low breakdown voltages. Significantly decreased electrical breakdowns in gases were attained in the vicinity of positively charged p-type ZnO NWs' tips. The applied voltages were less than 40 V. These experimental outcomes can be ascribed to the fact that Ag-doped ZnO NWs have an increased number of empty states below the Fermi level and because of the observed high curvature on the NWs' apexes. The calculated enhancement factors were 45 and 1.49×10^4 in the GIS based on n-type ZnO NWs and in the GIS based on p-type ZnO NWs, respectively. The novel GIS based on p-type ZnO NWs described here is inexpensive, simple in operation, consumes little power, and can be used for environmental monitoring and gas detection in industrial and living environments or for space applications.

1. Introduction

Gas sensors are used to prevent environmental contamination, to protect people from hazardous gases in an industrial environment, on board aircrafts and spacecrafts, and in living environments and to detect traces of different gases in space. Gas sensors identify the presence and concentration of gases or their mixtures, and they are divided into optical, acoustic, chemical, and electrical types.[1,2] A gas detector with superior performance, selectivity, sensitivity, reversibility, and durability is a goal worth achieving. In fact, an electrical sensor based on the physical phenomenon of gas ionization encompasses most of the requirements listed above, such as selectivity, reversibility, durability, and sensitivity.[3] These gas detectors are made of two conducting oppositely charged parallel plates. Breakdowns in gases occur owing to the voltage applied between two capacitive plates. The high electric field created inside gas ionization sensor (GIS) results in the ionization of gas, and the breakdown voltages are used as a fingerprint to identify the gases. However, one major disadvantage of these devices is the need for high applied voltages of approximately 1 kV.

With advances in nanotechnology, it became possible to grow nanostructured field emitters [nanowires (NWs)] and apply them to one of the capacitive plates of a gas sensor. The incorporation of NWs resulted in a considerable decrease in the applied voltages between the two

*Corresponding author: e-mail: spits_sv3@hotmail.com

ISSN 0914-4935

plates of a gas detector. GISs based on carbon nanotubes,[4] metallic NWs,[5–7] and semiconductor NWs and nanotubes[8–15] are the most studied. As a part of the ongoing investigation on the development of a sensitive odor sensor, our group has been conducting an investigation of GISs based on micro- and nanostructures.[5–7] However, it was observed that the fabricated gas detectors based on metallic NWs lose their sensitivity after several uses. This is ascribed to the fact that the high local electric fields created on NWs' pinnacles damage the tips of the silver and gold NWs. On the other hand, gas ionization sensors based on metal oxide (ZnO) NWs demonstrated improved durability and repeatability.[8,9] ZnO NWs have excellent chemical stability and can withstand high electric fields without structural degradation. However, ZnO NWs have a hexagonal structure, no curvature on the tips, and low electrical conductivity. This morphology leads to the generation of lower local electric fields on the apexes of NWs than in GISs based on metallic NWs. As a result, the applied voltages are higher in GISs based on ZnO NWs than in GISs based on metallic counterparts.

One of the solutions is to improve the electrical properties of ZnO NWs by introducing impurities into the NWs. In this work, electrochemical deposition was used to grow n-type and p-type ZnO NWs. This growth technique was chosen because it is an inexpensive and fast growth method with the potential to create uniform and large-area NWs, resulting in the strong adhesion of nanostructures to the substrate. Moreover, this growth method offers better control over the designed nanostructures and their physical properties than the hydrothermal growth technique.[16]

In this article, the effects of the incorporation into GIS of n-type or p-type ZnO NWs on the applied voltages, attained breakdown voltages in different amounts of gas in vacuum, and the detection of gas in air were studied.

2. Materials and Methods

2.1 Fabrication of ZnO NWs

The electrochemical growth of ZnO NWs was performed in a three-electrode cell in potentiostatic mode. The electrochemical cell included an auxiliary electrode (platinum wire gauze), a reference electrode (Ag/AgCl in saturated 4 M KCl with a potential drop of +0.24 V vs Normal Hydrogen Electrode), a working electrode (n^+-type silicon wafer), and an electrolyte, as shown in Fig. 1. One side of the silicon wafer (substrate) was covered with Al using a physical vapor deposition (PVD) technique followed by alloying at 450 °C for 30 min. To grow n-type ZnO NWs, an electrolyte contained two chemicals with equal concentrations of 5.4 mM diluted in deionized (DI) water, where the source of zinc ions was $Zn(NO_3)_2 \cdot 6H_2O$ and the source of hydroxide ions was $C_6H_{12}N_4$. Cationic doping of ZnO NWs was achieved by introducing silver ions into DI water ($AgNO_3$). An altered amount of $Zn(NO_3)_2 \cdot 6H_2O$ with $AgNO_3$ was added into the solution: 0.8% of the zinc ions' mass was replaced by the mass of silver ions, keeping the concentration of hexamethylenetetramine as before (5.4 mM).[17] Table 1 shows the constituents, their amounts inside the electrolyte, duration of the electrochemical process, temperature, and voltage applied to the electrochemical cell.

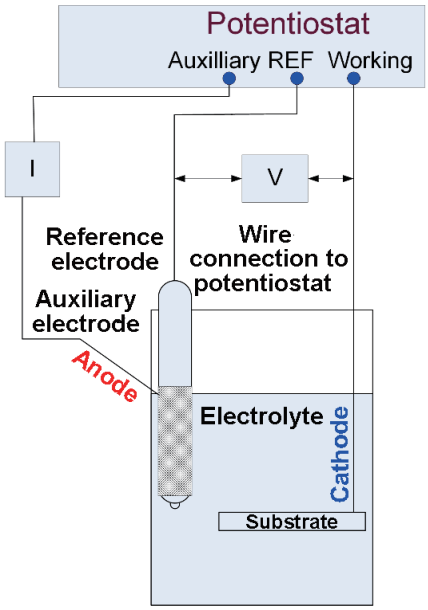

Fig. 1. (Color online) Electrochemical setup.

Table 1
Electrochemical parameters used to grow ZnO NWs integrated into GIS.

Conductivity type of ZnO NWs	Substrate	Chemicals	Concentration (g/l)	Applied voltage (V)	Growth temperature (°C)	Growth time (min)
n-type	n^+-type Si	$Zn(NO_3)2{\cdot}6H_2O$ $C_6H_{12}N_4$	1.606 0.757	−1.0	80	45
p-type	n^+-type Si	$Zn(NO_3)_2{\cdot}6H_2O$ $C_6H_{12}N_4$ $AgNO_3$	1.594 0.757 4.45×10^{-3}	−0.8	85	45

2.2 Fabrication of GISs with ZnO NWs

GIS is fabricated from two pieces of silicon wafer separated by an insulator, as demonstrated in Fig. 2. Silicon plates (n-type silicon wafer) act as electrodes of opposite polarities. One of the electrodes is covered by ZnO NWs, and the other one is coated by a microlayer of aluminum. An insulating spacer, i.e., a polypropylene ring with a resistivity of 10^{16}–10^{18} Ω·cm and a thickness of 60 μm, separates the two plates. Three openings in the spacer are created to facilitate gas flow between the two plates. The working area of the sensor (covered by NWs) is a circle of 21 mm diameter.

A staircase voltage sweep was applied to the sensor using Keithley 2400 single measurement units (SMUs). To ensure that the charging current due to the device capacitance is negligible, the sweep parameters were chosen as $\Delta V < 1$ V and $\Delta t = 50$ ms. All tests were performed in a vacuum chamber.

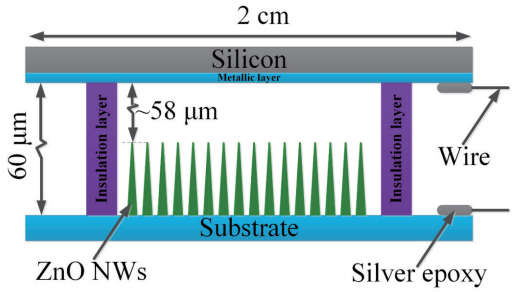

Fig. 2. (Color online) Schematic of GIS.

3. Results and Discussion

3.1 Simulation model and analysis of grown ZnO NWs

COMSOL simulations using a 3D electrostatic module demonstrated that NWs with sharp tips and highly dispersed distribution or with the diameters of the tips being smaller than the diameters of the bases lead to a high local electric field intensity in the vicinity of the NWs' apexes. NWs with the ratio of apex diameter to base diameter of 0.2 showed maximum intensity of the local electric field (geometry of the NWs used in simulations: d_{base} = 200 nm, d_{tip} = 40 nm, and $r_{curvature}$ = 10 nm). Also, a negligible screening effect in the created model was observed, as shown in Fig. 3. On the basis of previously conducted studies on the effect of growth conditions on the ZnO NWs' morphology,[17] ZnO NWs similar to the optimal simulated model were chosen for integration into GISs. These were ZnO NWs grown on n^+-type silicon: they had thin tips and wide base diameters. Also, nanoprotrusions were observed on the NWs' pinnacles. This fact suggested that these sharp nanotips on the NWs apexes will contribute to the augmentation of the local electric field.

The grown n-type and p-type ZnO NWs were analyzed by scanning electron microscopy (SEM), energy-dispersive X-ray spectroscopy (EDXS), and photoelectrochemical (PEC) cell measurements. Figure 4 shows SEM images of the electrochemically grown n-type and p-type ZnO NWs before integration into GISs. The grown n-type ZnO NWs reveal uneven surfaces on their pinnacles, as shown in Fig. 4(a). As for Ag-doped ZnO NWs, the geometry of NWs is the same as in the previous case; only the density of the nanofilm is increased, as demonstrated in Fig. 4(b). To investigate the chemical contents of the Ag-doped ZnO NWs, EDXS analysis was carried out. Figure 5 shows spectrum and mapping analyses. Spectrum analysis confirmed the presence of a small amount of silver inside the ZnO NWs, as shown in Fig. 5(a). Mapping analysis revealed uniform distributions of oxygen, zinc, and silver inside the nanofilm, as demonstrated in Fig. 5(b)–5(d). PEC cell testing was used to confirm the p-type conductivity of the grown Ag-doped ZnO NWs. The electrochemical cell used in the PEC cell measurement encompassed the electrolyte (5 mM KCl diluted in DI water), working electrode (Ag-doped ZnO NWs grown on n^+-type silicon), and reference electrode. It was operated in galvanostatic mode: current of 0 A was applied and potential was measured. The PEC cell was covered with aluminum foil to protect the tested sample inside the solution from light; only a small window was created, where white light (Model 21AC fiber optic illuminator, CO Edmund, Industrial optics) was applied. A substrate with doped ZnO NWs placed inside the electrolyte was allowed to face the small open window made in aluminum

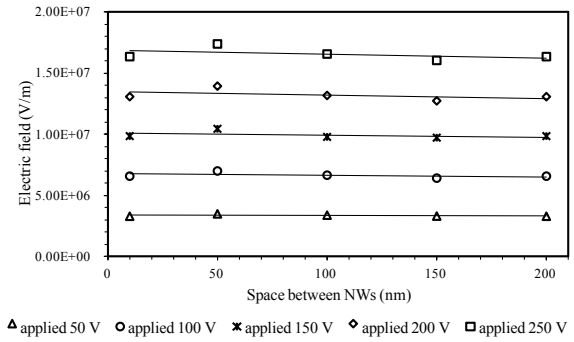

Fig. 3. Maximum electric field in vicinity of NWs' apexes at applied voltages from 50 to 250 V with steps of 50 V in 3D GIS model being composed of 9 NWs vs space between NWs.

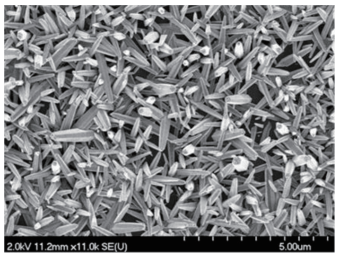

(a)

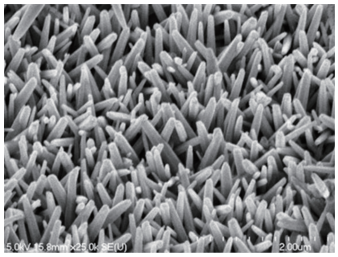

(b)

Fig. 4. (a) SEM image of n-type ZnO NWs grown on n^+-type silicon; (b) SEM image of Ag-doped ZnO NWs grown on n^+-type silicon.

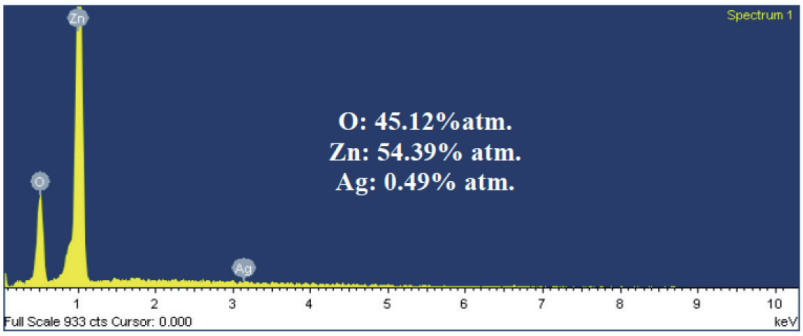

(a)

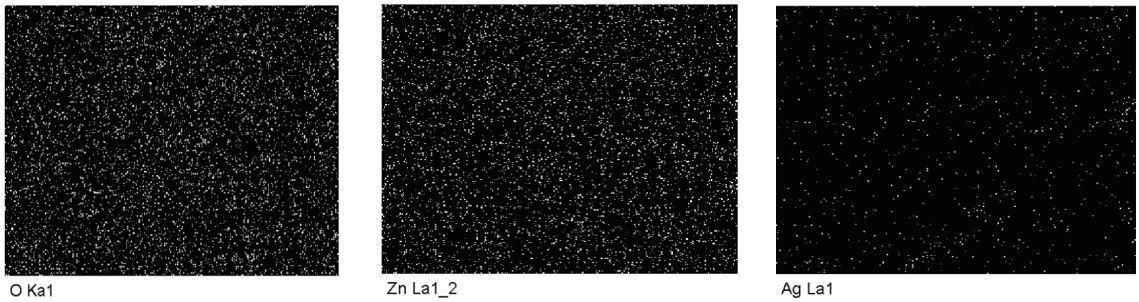

(b) (c) (d)

Fig. 5. (Color online) EDXS analysis of Ag-doped ZnO NWs: (a) spectrum analysis; mapping analysis: (b) distribution of oxygen, (c) distribution of zinc, and (d) distribution of silver in Ag-doped ZnO NWs.

foil. At first, the PEC system was standardized using known samples of n- and p-type silicon. Then, Ag-doped ZnO NWs were assessed. The detected voltage shift due to the applied light was 15 mV (V_{dark} = −160 mV and V_{light} = −145 mV). After this evaluation, n-type and p-type ZnO NWs were incorporated into GISs.

3.2 Assessment of GISs in low concentrations of argon

The fabricated GISs based on ZnO NWs were used to study the effect of gas concentration. The devices were operating in field emission (FE) and field ionization (FI) modes in Ar sub-Torr atmosphere, in the range of $0.01 < P < 0.25$ Torr, at room temperature (T = 300 K). In FE mode, the silicon plate with NWs is negatively charged in GIS. A large amount of electrons are emitted from the tips of the NWs, causing gas ionization, generating an avalanche of positive and negative charges moving in opposite directions and resulting in the gas breakdown. In FI mode, a silicon plate with NWs is positively charged in GIS. The NWs attract the gas electrons from the outer shell of gas molecules. A high nonlinear electric field near the NWs' apexes leads to gas ionization.[3,18–20]

Figure 6 shows the effect of concentration on the breakdown voltages in argon. First, the GIS based on n-type ZnO NWs was used in FI and FE modes. Lower breakdown voltages were detected

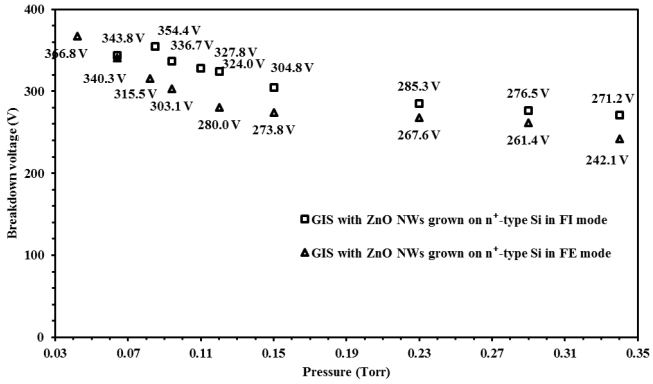

(a)

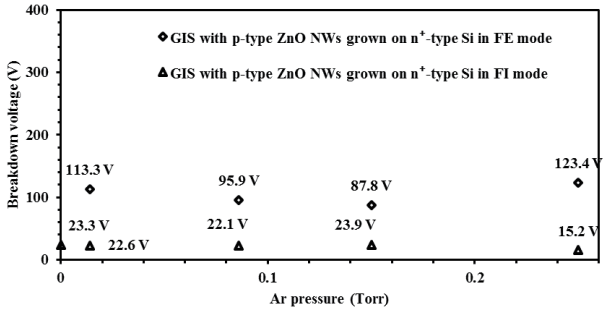

(b)

Fig. 6. Breakdown voltage vs Ar sub-Torr atmosphere is recorded using (a) the GIS based on n-type ZnO NWs grown on n^+-type Si in FE and FI modes and (b) the GIS based on p-type ZnO NWs grown on n^+-type Si in FE and FI modes.

when the gas sensor worked in FE mode than the voltages attained when the gas detector was working in FI mode, since n-type ZnO NWs have a high amount of electrons near the surface, as shown in Fig. 6(a). However, the difference in the breakdown voltages between the GISs operating in FE and FI modes was small (approximately 15 V) in view of the fact that ZnO NWs have a high amount of surface states. An increase in the breakdown voltage was detected at low gas pressures, as predicted by Paschen's law for uniform electric field and similar to the response of GIS with carbon nanotubes reported in Ref. 4.

Next, the GIS based on p-type ZnO NWs was tested under the same conditions. The observed breakdown voltages did not vary significantly with gas pressure. This can be ascribed to the fact that the breakdown was dominated by a nonlinear electric field near the NWs' pinnacles. The plasma created near the NWs' apexes leads to the generation of a conductive path between electrodes and reduces the sensitivity of the breakdown voltage to the amount of gas.[4] Also, a significant decrease in the breakdown voltages was observed in the GIS based on p-type ZnO NWs compared with the gas sensor based on n-type ZnO NWs. The reason is the creation of a high electric field by the p-type ZnO NWs, as this nanofilm has a higher aspect ratio and a lower energy band gap owing to p-type doping. Furthermore, the GIS based on p-type ZnO NWs demonstrated lower breakdowns in gas when it was operated in FI mode, because the p-type semiconductor NWs have a high amount of empty states above the Fermi energy level. Therefore, gas electrons had no difficulties in tunneling into p-type NWs.

3.3 Detection of different concentrations of gases in vacuum

The effect of concentration on the breakdown voltages of argon, helium, oxygen, and nitrogen is discussed in this section. Ar, He, N_2, and O_2 were introduced into the vacuum chamber (10^{-5} Torr) and detected by the GIS based on p-type ZnO NWs operating in FI mode. Figures 7(a)–7(d) show the *I–V* characteristics of the GIS. The Ohmic region, where the field strength is small and current flows because of the existing radiation-generated electron–ion pairs, transformed into a field-limited region, where a sharp increase in current is observed. Only a slight difference in the breakdown voltage due to the increased gas concentration was observed in Figs. 7(a)–7(d). A rapid voltage decrease after breakdown with increasing current was observed in 0.096 Torr nitrogen pressure and in low oxygen concentrations, as shown in Figs. 7(c) and 7(d). This happened because a positive corona discharge in the vicinity of the positively charged NWs' pinnacles occurred once the breakdown voltage was reached, which resulted in the glow of the corona. The glow discharge manifested owing to the emission of photons during the recombination of high-energy electrons and positive gas ions. The emitted photons energized the electrons in other gas molecules and the electrons gained sufficient energy to leave the gas atoms. Hence, current increased and voltage decreased. Figure 7(e) summarizes the effect of different gas concentrations (Ar, N_2, He, and O_2) on breakdown voltages in GIS. Experimental outputs showed a negligible difference between breakdowns in high concentrations of gases. Because of the highly nonlinear electric fields in the vicinity of the NWs' apexes, the breakdowns for different gases were almost the same. However, different breakdown voltages were obtained in low gas concentrations (10^{-5} Torr). The breakdowns of different gases in GIS confirmed the uniqueness and independence of the outputs from the gas concentration. Therefore, a gas can be identified by breakdown voltage in GIS. The voltages applied to GIS were less than 40 V; thus, this gas detector can be used as a portable device with batteries installed.

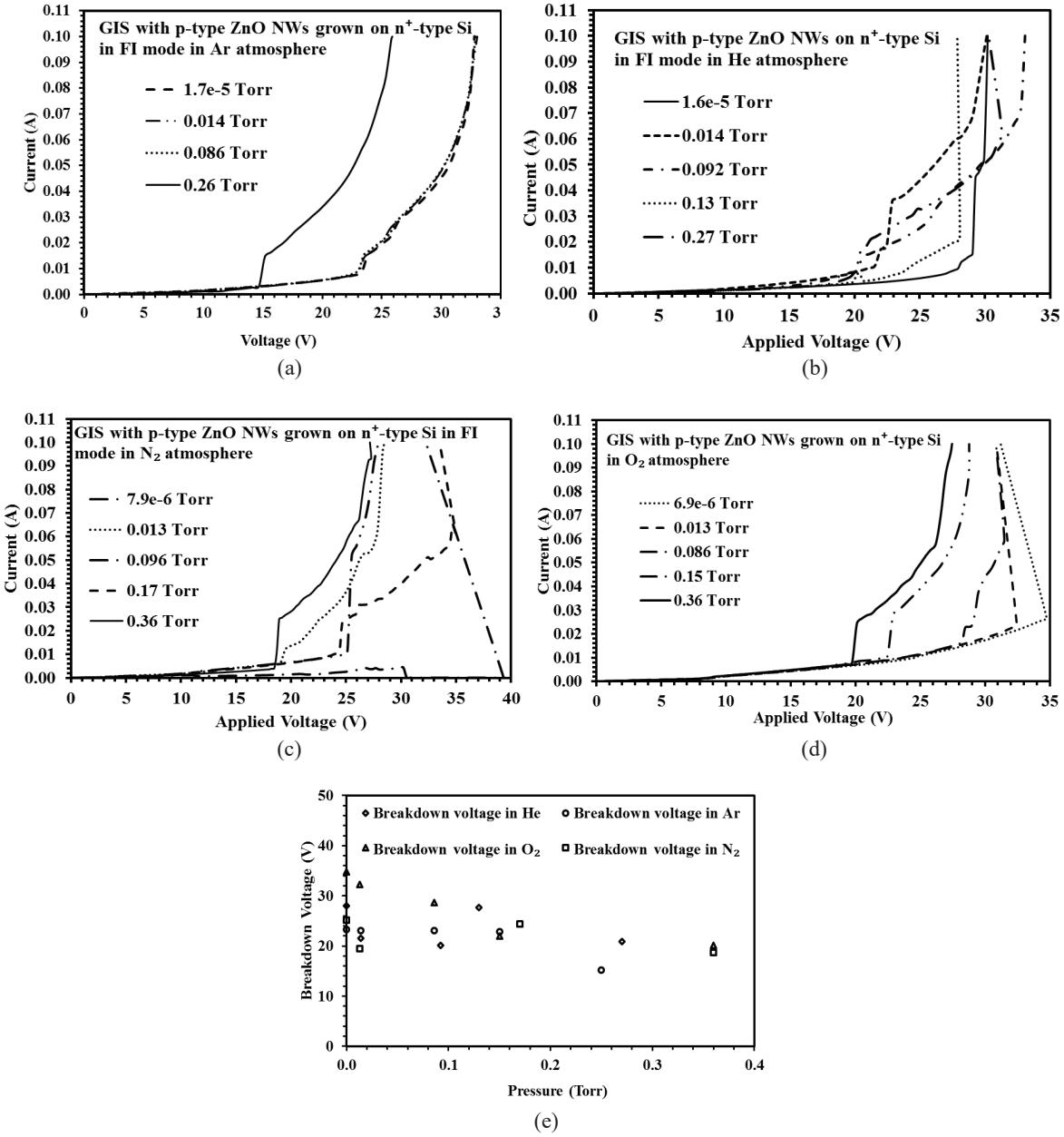

Fig. 7. *I–V* characteristics of the GIS based on p-type ZnO NWs grown on n^+-type Si in FI mode for the detection of different concentrations of gases in vacuum: (a) Ar, (b) He, (c) N_2, and (d) O_2. (e) Breakdown voltages vs different gas pressures.

The repeatability of GIS was good; the standard deviation was less than 1.0 V. All experiments were repeated 3 times for each gas, for each gas pressure, and for each test (each GIS was used a minimum of 108 times for gas detection).

After that, the effect of different gases at constant pressure on the current generated in the GIS based on p-type ZnO NWs was studied. The currents created in different gases (Ar, He, N_2, and O_2) and at a constant gas pressure of 0.01 Torr were examined at applied voltages of 1 and 5 V. Variations of the current in the field-limited region were observed owing to the dissimilar mobilities of gas ions. Gas with a high mobility of ions produced high current in the GIS compared with gas

with a low mobility of ions. Table 2 shows the experimental results of this investigation. As can be seen, the formed ionic currents at applied 5 V (between 35.8 and 36.7 μA) were hundreds of times higher than the generated currents at applied 1 V (between 0.116 and 0.178 μA). At both applied voltages, the smallest current was generated in the He sub-Torr atmosphere. Moreover, the lowest generated current at low electric fields was obtained in helium, because this gas has the highest ionization energy (24.5874 eV) compared with oxygen (13.6181 eV), nitrogen (14.5341 eV), and argon (15.7596 eV).[21] As known, the field-limited current depends on the ionization probability of the gas.[19] Furthermore, the distinguishable values of generated currents in different gaseous atmospheres make it possible to fingerprint the gases using a sensor at the biased voltage of 5 V.

3.4 Detection of gas leakage in air

Here, we report on the detection of a gas-air mixture by the GIS based on p-type ZnO NWs, where a silicon plate with NWs was configured as the anode. Gas flow in air in an open vacuum chamber was regulated by a mass flow controller (120 units applied). Figure 8 shows the *I–V* characteristics of the GIS for different gas-air mixtures. The smallest breakdown voltage of 17 V at a generated current of 13 mA was detected in the He-air mixture, as shown in Fig. 8. This can be attributed to the fact that He has the smallest gas ion radius compared with the other gases investigated and, therefore, it has a high mobility as a consequence of the large mean free path.[22] As air consists of 78% nitrogen, the detected breakdown voltage and generated current at breakdown were similar in air and N_2-air mixture. Moreover, the breakdown voltages in air and in the N_2-air mixture as well as in Ar-air and O_2-air mixtures were similar. However, the amounts of generated

Table 2
Field-limited current detected in GIS based on p-type ZnO NWs at applied bias voltages of 1 and 5 V and at a gas pressure of 0.01 Torr.

Gas	Ar		O_2		He		N_2	
Bias voltage (V)	1	5	1	5	1	5	1	5
Current (μA)	0.152	36.6	0.152	36.7	0.116	35.8	0.178	36.4

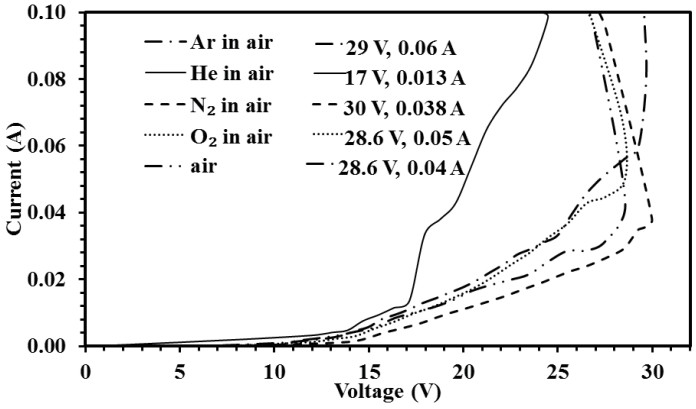

Fig. 8. *I–V* characteristics of the GIS based on p-type ZnO NWs grown on n^+-type Si in FI mode used for the detection of gas traces in air.

currents at breakdown were different in these gas mixtures. The highest current was observed in the Ar-air mixture followed by the obtained currents in the O_2-air mixture and N_2-air gaseous atmosphere.

3.5 Estimation of field enhancement factor

The field enhancement factor was calculated in GISs based on n-type or p-type ZnO NWs, where a silicon plate with NWs was arranged as the cathode, using the *I–V* characteristics of GISs under vacuum condition ($P = 2.0 \times 10^{-5}$ Torr). To estimate the field enhancement factor, the slope in the linear region of the generated dark discharge current was used. In this region, the ionization-induced current is negligible, and the slope represents conductivity. Figure 9(a) shows the *I–V* curve of the GIS based on n-type ZnO NWs with an identified slope in the linear region, which demonstrates a conductivity (G) of 3.7×10^{-10} Ω^{-1}. The enhancement factor (γ) was obtained as $\gamma = G/G_0 = 45$ following Ref. 5 and using the conductivity of the GIS with two parallel plates ($G_0 = 8.3 \times 10^{-12}$ Ω^{-1}).

In the case of the GIS based on p-type ZnO NWs, the linear region was negligible, and conductivity was obtained from the linear approximation of the experimental curve. The obtained conductance was 1.17×10^{-7} Ω^{-1}, as shown in Fig. 9(b), and the calculated enhancement factor was around 14096. To confirm this evaluated value, we used the Fowler-Nordheim tunneling equation to estimate the field enhancement factor. The effective area of the electron emission was derived from the SEM images. There are 82 NWs with diameters between 30 and 50 nm per area of 10^6 nm². The effective number of NWs on the surface of GIS is around [346.36×10^{12} nm² (area of the active surface)/(10^6 nm²)] × 82 = 2.84×10^{10}. Assuming that all areas of the tip emit electrons, the calculated emitting area is about $2.84 \times 10^{10} \times (20\text{ nm})^2 \times \pi = 35.6885 \times 10^{12}$ (nm²) = 35.6885 (mm²). Figure 10(a) shows that the maximum electric field (1.64×10^3 V/mm) created a current density of 1.44 mA/mm². Figure 10(b) shows the graph $\ln(J/E^2)$ vs $1/E$, where the function $\ln(J/E^2)$ is derived from the Fowler–Nordheim tunneling equation[23] as

$$\ln[J/E^2] = -[v(f)b\phi^{3/2}]/(\gamma E) + \ln\{(\alpha\gamma^2)/[(1.07)^2\phi]\}, \quad (1)$$

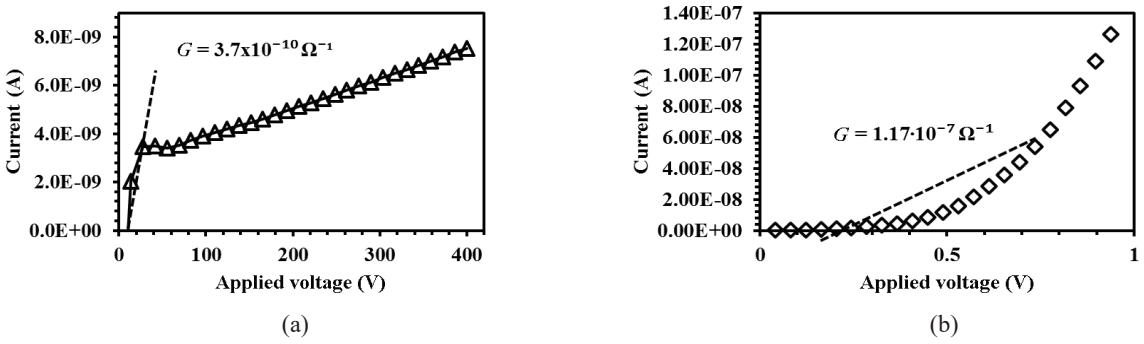

Fig. 9. (a) Dark current in GIS with n-type ZnO NWs as cathode in low air pressure ($P = 2.0 \times 10^{-5}$ Torr) and (b) dark current in GIS with p-type ZnO NWs as cathode in low air pressure ($P = 3.4 \times 10^{-5}$ Torr).

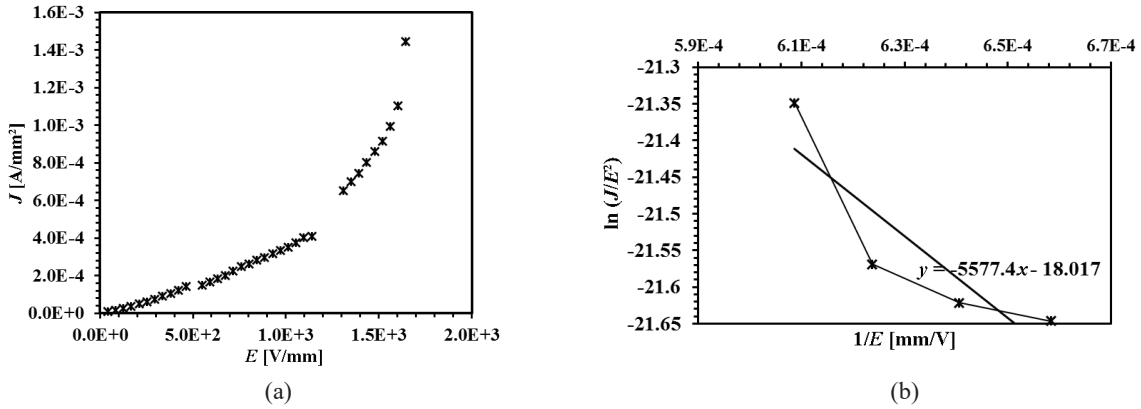

Fig. 10. (a) *J–E* curve generated in the GIS based on p-type ZnO NWs grown on n^+-type Si showing the electric field of 1.64 kV/mm for an emission current density of 1.44 mA/mm² and (b) Fowler-Nordheim plot $\ln(J/E^2)$ vs $1/E$ corresponding to (a).

where the first term ($[v(f)b\phi^{3/2}]/\gamma$) is the slope of the curve, and it was used to estimate the field enhancement factor of 14941.8 assuming that the ZnO work function is 5.3 eV and $v(f)$ is 1. This field enhancement factor is similar to the one that was calculated using the conductance slope (γ = 14096). A similar enhancement factor of 1.4×10^4 was reported by Wang *et al.* for ZnO nanobelts.[15]

4. Conclusions

P-type and n-type ZnO NWs electrochemically grown on n^+-type Si have been chosen as the active material for GISs, as a result of simulation studies on the most appropriate morphology of NWs in terms of the highest local electric field and negligible screening effect. Gas detectors based on n-type or p-type ZnO NWs were tested in Ar. The GIS based on p-type ZnO NWs showed low breakdown voltages in Ar sub-Torr pressures because of the increased conductivity in Ag-doped ZnO NWs. Furthermore, the gas detector based on p-type ZnO NWs configured as the anode was able to identify different gases (Ar, He, N_2, and O_2) by recognizing the produced ionic current. Moreover, the detection of gas mixtures in air illustrated the capability of the novel gas sensor to detect gases that have different physical properties [ionic energy and radius (such as He)] compared with gaseous elements in air. Finally, the estimated enhancement factors were 45 and 1.49×10^4 in the GIS based on n-type ZnO NWs and the GIS based on p-type ZnO NWs, respectively.

Acknowledgements

The authors would like to thank the Natural Sciences and Engineering Research Council (NSERC) and the Faculty of Engineering & Computer Science, Concordia University (ENCS) for funding this work.

References

1 X. Liu, S. Cheng, H. Liu, S. Hu, D. Zhang, and H. Ning: Sensors **12** (2012) 9635.
2 P. Lv, Z. A. Tang, J. Yu, F. T. Zhang, G. F. Wei, Z. X. Huang, and Y. Hu: Sens. Actuators, B **132** (2008) 74.
3 J. M. Meek and J. D. Craggs: Electrical Breakdown of Gases, eds. N. F. Mott and Sir E. Bullard (Oxford University Press, London, 1953) p. 80.
4 A. Modi, N. Koratkar, E. Lass, B. Wei, and P. M. Ajayan: Nature **424** (2003) 171.
5 R. B. Sadeghian and M. Kahrizi: Sens. Actuators, A **137** (2007) 248.
6 R. B. Sadeghian and M. Kahrizi: IEEE Sens. **8** (2008) 161.
7 N. Azmoodeh, N. Chivu, R. B. Sadeghian, and M. Kahrizi: Proceedings of EUROCON 2009 (IEEE, 2009) p. 1231.
8 L. Liao, H. B. Lu, M. Shuai, J. C. Li, Y. L. Liu, Z. X. Shen, and T. Yu: Nanotechnology **19** (2008) 1.
9 H. Wang, C. Zou, C. Tian, L. Zhou, Z. Wang, and D. Fu: Nanoscale Res. Lett. **6** (2011) 534.
10 H. Nguyen, C. T. Quy, N. D. Hoa, N. T. Lam, N. V. Duy, V. V. Quang, and N. V. Hieu: Sens. Actuators, B **193** (2014) 888.
11 D. Yan, M. Hu, S. Li, J. Liang, Y. Wu, and S. Ma: Electrochimica Acta **115** (2014) 297.
12 J. Y. Kim, S.-Y. Jo, G.-J. Sun, A. Katoch, S.-W. Choi, and S. S. Kim: Sens. Actuators, B **192** (2014) 216.
13 P. Afzali, Y. Abdi, and E. Arzi: Sens. Actuators, B **195** (2014) 92.
14 R. B. Sadeghian and M. S. Islam: Nat. Mater. **10** (2011) 135.
15 W. Wang, B. Zeng, J. Yang, B. Poudel, J. Huang, M. J. Naughton, and Z. Ren: Adv. Mater. **18** (2006) 3275.
16 H. Huang, P. Xu, D. Zheng, C. Chen, and X. Li: J. Mater. Chem. A **3** (2015) 6330.
17 S. Spitsina and M. Kahrizi: Adv. Sci. Eng. Med. **6** (2014) 553.
18 E. W. Müller and T. T. Tsong: Field Ion Microscopy: Principles and Applications (Elsevier Publishing Company, Ltd., New York, NY, 1969) p. 10.
19 Y. Ohno, S. Nakamura, and T. Kuroda: Jpn. J. Appl. Phys. **17** (1978) 2013.
20 T. T. Tsong: Physs Today (May, 1993) 24.
21 Ionization Energies (eV) of Atoms and Ions, http://dept.astro.lsa.umich.edu/~cowley/ionen.htm (accessed April 2015).
22 WebElements, http://www.webelements.com/ (accessed April 2015).
23 R. G. Forbes: J. Vac. Sci. Technol., B **26** (2008) 209.